AGU ADVANCING EARTH AND SPACE SCIENCES

Geophysical Research Letters

RESEARCH LETTER
10.1029/2025GL115385

Phase Relations in the $MgSiO_3$ System Associated With Hot Mantle Upwelling Across the 660 km Depth

Artem Chanyshev[1], Narangoo Purevjav[1,2], Dmitry Bondar[1], Hu Tang[1,3], Hongzhan Fei[1,4], Lin Wang[1,5], Fei Wang[1], Eun Jeong Kim[1,6], Dan Liu[1,7,8], Takayuki Ishii[1,9], Shrikant Bhat[10], Robert Farla[10], and Tomoo Katsura[1]

[1]Bayerisches Geoinstitut, University of Bayreuth, Bayreuth, Germany, [2]School of Earth and Environmental Sciences, Seoul National University, Seoul, Korea, [3]State Key Laboratory of High Pressure and Superhard Materials, College of Physics, Jilin University, Changchun, China, [4]School of Earth Sciences, Zhejiang University, Hangzhou, China, [5]Institute of Geochemistry, Chinese Academy of Science, Guiyang, China, [6]Department of Geoenvironmental Sciences, Kongju National University, Gongju, Korea, [7]Gemmological Institute, China University of Geosciences, Wuhan, China, [8]State Key Laboratory of Geological Processes and Mineral Resources, China University of Geosciences, Wuhan, China, [9]Institute for Planetary Materials, Okayama University, Misasa, Japan, [10]Deutsches Elektronen-Synchrotron DESY, Hamburg, Germany

Abstract The phase transformations of $MgSiO_3$ bridgmanite control the structure, dynamics and chemistry of the Earth's mantle. Formation of bridgmanite occurs at a depth of about 660 km causing the strong and abrupt seismic discontinuity. Previous experimental studies have revealed that this discontinuity is caused by ringwoodite dissociation in the average mantle. However, the cause of the 660-km seismic discontinuity beneath hotspots remains unclear. Here we determine the phase relations in the $MgSiO_3$ system near the 660-km seismic discontinuity conditions. At 2,200–2,350 K with decreasing pressure, $MgSiO_3$ bridgmanite first transforms to akimotoite and then to garnet. The akimotoite-bridgmanite boundary has almost no temperature dependence, whereas the garnet–akimotoite transition has a very steep positive boundary slope. Based on these slopes, we calculated the garnet–bridgmanite boundary slope. Depending on the temperature regime, the akimotoite-bridgmanite or the garnet–bridgmanite transition may occur in ascending plume beneath hotspots near the 660 km depth.

Plain Language Summary This study determines phase relations in the $MgSiO_3$ system at the upwelling plume zone conditions near the 660-km seismic discontinuity (D660). The $MgSiO_3$ system was selected since the most abundant mineral in the Earth's lower mantle—bridgmanite—contains about 90% of this component. The D660—is a boundary between the lower mantle and transition zone in the Earth. The D660 is usually attributed to the ringwoodite dissociation to bridgmanite and ferropericlase in peridotite. The D660 is elevated beneath hot plume zones, and this elevation cannot be explained by the ringwoodite dissociation. We used the most reliable experimental technique to find the interpretation of this phenomenon. Our results indicate that the D660 elevation beneath plume zones can be caused by the akimotoite-bridgmanite transition if plume temperature is low or by the garnet–bridgmanite transition if plume temperature is high. The akimotoite-bridgmanite transition has no effect on mantle geodynamics, whereas the garnet–bridgmanite transition may accelerate plume rising.

Key Points:

- Phase relations in the $MgSiO_3$ system were investigated at 2,200–2,350 K and 17.4–20.3 GPa using multi-anvil with in situ X-ray diffraction
- At 2,200–2,350 K with decreasing pressure, $MgSiO_3$ bridgmanite first transforms to akimotoite and then to garnet
- Beneath hotspots, the 660-km seismic discontinuity elevation can be caused by the akimotoite-bridgmanite or garnet-bridgmanite transition

Supporting Information:

Supporting Information may be found in the online version of this article.

Correspondence to:

A. Chanyshev,
artem.chanyshev@uni-bayreuth.de

Citation:

Chanyshev, A., Purevjav, N., Bondar, D., Tang, H., Fei, H., Wang, L., et al. (2025). Phase relations in the $MgSiO_3$ system associated with hot mantle upwelling across the 660 km depth. *Geophysical Research Letters*, *52*, e2025GL115385. https://doi.org/10.1029/2025GL115385

Received 17 FEB 2025
Accepted 21 AUG 2025

1. Introduction

The 660-km seismic discontinuity (D660) is a global feature of the Earth's mantle and provides insights into mantle structure and dynamics. The D660 is usually attributed to the dissociation of ringwoodite (Rwd) to bridgmanite (Bdm) and periclase (Per) (Chanyshev et al., 2022; Ishii et al., 2019). Many seismic studies have shown that the D660 is elevated in upwelling hot plume zones and depressed in cold subduction regions (Houser & Williams, 2010). Depressed D660 beneath cold subduction zones is interpreted by the akimotoite (Aki)–bridgmanite transition (Chanyshev et al., 2022). Elevated D660 in hot plume zones was previously interpreted by the negative Clapeyron slope (dP/dT) of the Rwd dissociation (Irifune et al., 1998; Ishii et al., 2011; Ito & Takahashi, 1989). However, our recent experimental study revealed that the Rwd dissociation boundary in Mg_2SiO_4 has an almost neutral Clapeyron slope (Chanyshev et al., 2022), and therefore it cannot cause a significant change in the seismic discontinuity depth. Thus, an alternative explanation for the D660 elevation in plume zones is needed.

A possible interpretation is the majorite garnet (Grt)-Bdm transition. Previous experimental and computational studies have shown that this transition in the $MgSiO_3$ system occurs at slightly lower pressures than the Rwd dissociation at plume conditions near the D660 (Hernández et al., 2015; Hirose et al., 2001; Ishii et al., 2011; Kulka et al., 2020; Sawamoto, 1987; Yu et al., 2011; Yusa et al., 1993). Hence, the Grt-Bdm transition could be responsible for the D660 elevation in plume zones, although it has a positive Clapeyron slope.

As we have postulated in previous studies, a combination of the multi-anvil technique with in situ X-ray diffraction gives reliable high P–T phase relations data (Chanyshev et al., 2022; Ishii et al., 2022). Among the previous experimental studies performed in multi-anvil apparatus using in situ X-ray diffraction, the Grt-Bdm boundary was determined only by very few experiments (Hirose et al., 2001), which is insufficient to conclude its contribution to the D660 in plume zones. Our recent experimental studies showed that the phase transition boundary at high P–T conditions should be determined by balancing the normal and reverse reactions of a phase transition in situ (Chanyshev et al., 2022; Ishii et al., 2022, 2023). Therefore, it is crucial to systematically examine the Grt-Bdm phase transition boundary using our established methodology.

2. Methods

2.1. Preparation of Starting Materials

$MgSiO_3$ enstatite glass was used as a starting material. The glass was prepared from reagent grade oxides of SiO_2 and MgO. These oxides were heated at 1,270 K for 16 hr to remove adsorbed water and then mixed by grounding with acetone in an agate mortar for 1 hr. The resulting mixture was heated to 1,873 K for 1 hr and quenched into cold water. After that, obtaining glass was ground with acetone in an agate mortar for 1 hr.

Reagent-grade MgO powder mixed with diamond powder (10:1 weight %) to prevent grain growth was used as a pressure marker for the in situ X-ray diffraction experiments. Magnesium oxide powder was heated at 1,270 K for 16 hr to remove adsorbed water prior to weighing. A mixture of MgO and diamond was ground with acetone in an agate mortar for 1 hr. Using a mixture of MgO and diamond as a pressure marker may introduce uncertainties in pressure determination using MgO at low temperatures due to the formation of a load-bearing framework. However, since the fraction of diamond is low (≈10 volume %), it is unlikely that such a framework was formed. Furthermore, the temperature in this study is sufficiently high (>2,000 K) to weaken any framework that may have formed. Therefore, the influence of adding diamond to MgO on pressure should be minimal.

Both the $MgSiO_3$ enstatite glass and the MgO + diamond mixture were compressed to 5 GPa and heated to 1,000 K for 1 hr using the 10-MN Kawai type multi-anvil press at the Bayerisches Geoinstitut, University of Bayreuth to make the sintered samples. Tungsten carbide anvils with 15-mm truncated edge lengths were used to generate high pressure together with a Cr-doped MgO octahedron with a 25-mm edge length as the pressure medium. The inside of the pressure medium consisted of a stepped cylindrical graphite heater and ZrO_2 thermal insulator. A Mo foil (50-μm thick) was used as the sample capsule. The temperature was measured on the surface of the capsule using a $W_{97}Re_3$−$W_{75}Re_{25}$ thermocouple.

The recovered samples were analyzed using a micro-focused X-ray diffractometer (Brucker AXS Discover 8) with a two-dimensional solid-state detector (SSD) (VANTEC500) and micro-focus source (IμS) with Co-Kα radiation operated at 40 kV and 500 μA. The synthesized samples were cut into discs 1.0 mm in diameter and 0.5 mm in thickness. The sintered MgO was cut into discs 1.0 and 1.5 mm in diameter and 0.5 mm in thickness.

2.2. In Situ X-Ray Diffraction Experiments

The phase relations in the $MgSiO_3$ system at 2,200–2,350 K were determined at the DESY synchrotron radiation facility (Hamburg, Germany). The experiments were performed at beamline P61b at DESY using the 3 × 5-MN six-axis multi-anvil press (Farla et al., 2022). X-ray diffraction patterns were collected for 150–300 s for the pressure marker and 300–3,000 s for the sample using a Ge SSD with a 4,096-channel analyzer. The SSD analyzer was calibrated using the X-ray fluorescence lines of ^{57}Co and ^{133}Ba before the measurements. The diffraction angle (2θ) was calibrated before each experiment with a precision of 0.0003° using MgO as a standard.

Two different types of cell assemblies were used in this study similar to Chanyshev et al. (2024). The first type of cell assembly consisted of an MgO + Cr_2O_3 octahedral pressure medium, a cylindrical boron-doped diamond (BDD) heater, ZrO_2 thermo-insulators and TiC electrodes (Figure S1a in Supporting Information S1). The sample

and pressure marker were isolated from the BDD heater by MgO sleeves. The temperature was measured using a $W_{97}Re_3$–$W_{75}Re_{25}$ thermocouple located in the center of the assembly and was separated from the heater by Al_2O_3 tubes. The second type of cell assembly consisted of an MgO + Cr_2O_3 octahedral pressure medium, a strip-type BDD heater and tetragonal MgO prism with round corners (Figure S1b in Supporting Information S1). Temperature was also measured using a $W_{97}Re_3$–$W_{75}Re_{25}$ thermocouple located in the center of the furnace between the pressure marker and the sample disks. The thermocouple, sample and pressure marker were isolated from the BDD stripes with the MgO prism. In both types of assemblies, we isolated the BDD heater from the pressure medium with MgO sleeves to prevent the reduction of Cr_2O_3. We carefully monitored the resistance between the heater and the thermocouple before and after heating to confirm the reliability of the temperature measurements. The pressure effect of the thermoelectromotive force of the thermocouple was corrected using the equations determined by Nishihara et al. (2020) after the experiments.

The incident X-ray beam collimated to dimensions of 30–50 μm horizontally and 200–300 μm vertically was directed at the sample through the gaps between the second-stage anvils. All of the experiments were carried out with a press oscillation around the vertical press axis between 0° and 6° during the X-ray diffraction measurement to suppress intensity heterogeneities of the diffracted peaks due to possible grain growth at high temperature. The pressure was obtained from the MgO unit cell volumes using the equations of state proposed by Tange et al. (2009) based on the third-order Birch-Murnaghan (3BM) and Vinet equations of state. To calculate the MgO unit cell volumes, we usually used eight diffraction peaks (111, 200, 220, 311, 222, 400, 420, 422), which produce relatively high precision in pressure (Chanyshev et al., 2022; Ishii, Huang et al., 2018; Ishii et al., 2022).

3. Results and Discussion

3.1. Phase Transition Boundaries

In this study, we determined Aki-Bdm and Grt-Aki phase transition boundaries in the $MgSiO_3$ system at 2,200–2,350 K using advanced multi-anvil techniques with in situ X-ray diffraction (Table S1 in Supporting Information S1). The Aki-Bdm boundary was determined mostly using our previously established technique (Chanyshev et al., 2022; Ishii et al., 2022), except for one data point at 2,245 K. For the Grt-Aki transition, we initially considered using our previously established technique as well. However, we encountered some difficulties determining the phase transition boundary between Aki and Grt, since the transition between these phases occurred extremely fast (full transformation from Aki to Grt during the data acquisition of pressure marker + sample = 8 min), and stable pressure-temperature conditions for the coexistence of Aki and Grt could not be achieved. Therefore, this phase transition was determined by the abrupt disappearance of one phase and the appearance of another one.

In the temperature range of 2,200–2,350 K, the Aki-Bdm boundary was determined at 20.2–20.3 GPa with a step of ≈50 K. At 2,245 K, the phase transition was determined by the abrupt disappearance of Bdm and the appearance of Aki with decreasing pressure (Figure 1a). At 2,192, 2,300 and 2,354 K, the phase transition was determined by the relative change in intensity of the Aki and Bdm diffraction patterns (Figure 1c). The resulting Clapeyron slope of the Aki-Bdm boundary at 2,200–2,350 K was determined to be slightly negative at around −0.6 MPa/K (Figure 2a). To obtain a more accurate phase diagram, we combined our data with our previous experimental data on the Aki-Bdm transition boundary at lower temperatures of 1,250–2,085 K (Chanyshev et al., 2022). The resulting Aki-Bdm transition boundary from 1,250 to 2,350 K is shown in Figure 2b. The slope of this boundary gradually changes from −8.1 MPa/K at low temperatures below 1,300 K to −0.6 MPa/K at temperatures above 2,200 K.

The Grt-Aki boundary was found at 17.4–18.7 GPa at 2,200–2,350 K. At ≈ 2,350 K, the phase transition was determined by the abrupt disappearance of Aki and the appearance of Grt with a significant decrease in pressure from 19.84 to 18.42 GPa (Figure 1b). Furthermore, the Aki-Grt phase transition was observed by the abrupt disappearance of Aki and appearance of Grt with a decrease in pressure from 18.61 to 18.48 GPa during heating from 2,295 to 2,348 K. At ≈2,187 K, we observed the abrupt disappearance of Bdm instead of Aki and the appearance of Grt with a significant decrease in pressure from 19.22 to 17.13 GPa. Although Aki is a stable phase at 19.22 GPa and 2,187 K, we observed only Bdm diffraction patterns. We consider that Bdm is metastable at these conditions and accept the assumption that the Aki-Grt transition at this temperature occurs at the same pressure as determined for the Bdm-Grt transition. The Clapeyron slope of the Grt-Aki boundary was estimated to

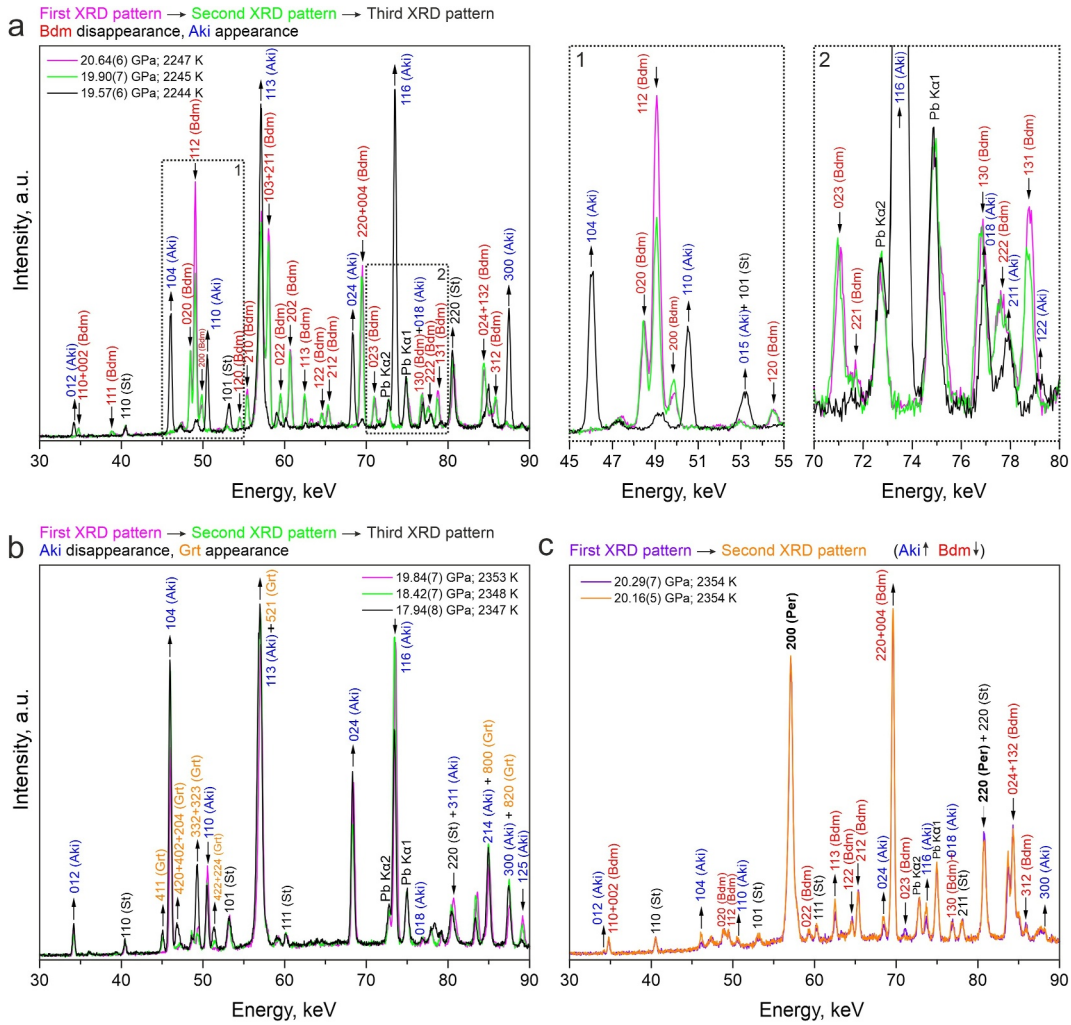

Figure 1. Accurate phase identification by means of in situ X-ray diffraction in a multi-anvil press. (a) Disappearance of Bdm and appearance of Aki at 2,245–2,247 K during decreasing pressure from 20.64(6) to 19.57(6) GPa. (b) Disappearance of Aki and appearance of Grt at 2,347–2,353 K during a pressure decrease from 19.84(7) to 17.94(8) GPa. (c) Change in intensity ratio between Aki and Bdm at 2354 K and 20.29(7)–20.16(5) GPa. The numbers above the peaks indicate the Miller indexes of Aki, Bdm, Grt, St and Per. The upward and downward arrows indicate peaks with increased and decreased intensities in the second and third diffraction patterns, respectively. The fluorescence lines of Pb Kα and Kβ are shown by the Siegbahn notation.

be 8.8 MPa/K (Figure 2). The triple Aki-Bdm-Grt point is located at approximately 20.2 GPa and 2,530 K by linear extrapolation of the Aki-Bdm and Grt-Aki boundaries above 2,200 K (Figure 2).

Although we did not experimentally determine the Grt-Bdm phase transition boundary, we can estimate the slope of this boundary from those of the Aki-Bdm and Grt-Aki boundaries. The slope of a phase boundary is equal to the ratio of the entropy change (ΔS_{tr}) to the volume change (ΔV_{tr}) associated with the phase transition according to the Clausius–Clapeyron relation: $dP/dT = \Delta S_{tr}/\Delta V_{tr}$. The Clausius–Clapeyron relations of Aki-Bdm, Grt-Aki and Grt-Bdm boundaries can be described as follows:

$$(dP/dT)_{\text{Aki-Bdm}} = \Delta S_{\text{Aki-Bdm}}/\Delta V_{\text{Aki-Bdm}} = (S_{\text{Aki}} - S_{\text{Bdm}})/\Delta V_{\text{Aki-Bdm}} \quad (1)$$

$$(dP/dT)_{\text{Grt-Aki}} = \Delta S_{\text{Grt-Aki}}/\Delta V_{\text{Grt-Aki}} = (S_{\text{Grt}} - S_{\text{Aki}})/\Delta V_{\text{Grt-Aki}} \quad (2)$$

$$(dP/dT)_{\text{Grt-Bdm}} = \Delta S_{\text{Grt-Bdm}}/\Delta V_{\text{Grt-Bdm}} = (S_{\text{Grt}} - S_{\text{Bdm}})/\Delta V_{\text{Grt-Bdm}} \quad (3)$$

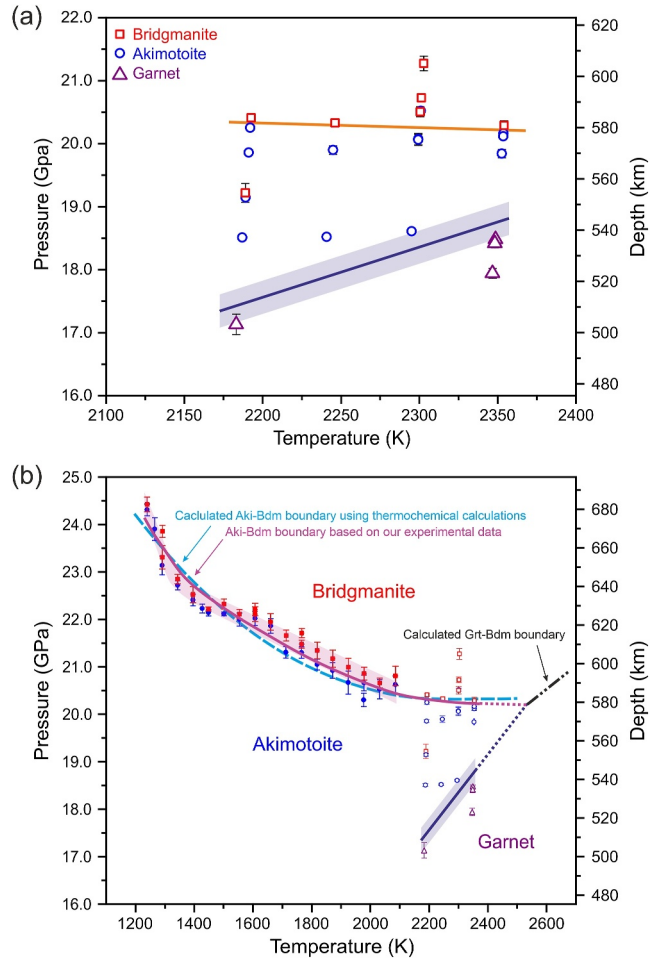

Figure 2. Phase relations in the $MgSiO_3$ system. (a) Aki-Bdm and Grt-Aki phase transition boundaries determined in the current study at 2,150–2,350 K and 17–21 GPa. (b) $MgSiO_3$ phase diagram at 1,200–2,600 K and 17–25 GPa. Red squares, blue circles, and purple triangles indicate the P–T conditions of Bdm, Aki, and Grt stability fields, respectively. Open and filled symbols are from the current study and from Chanyshev et al. (2022), respectively. Pressures were determined from the MgO unit-cell volumes using the Birch–Murnaghan and Vinet equations of state from Tange et al. (2009). Error bars result from the pressure uncertainty of the MgO equation of state suggested by Tange et al. (2009). The temperatures and pressures were corrected based on the pressure effects on the thermoelectromotive force of a $W_{97}Re_3$–$W_{75}Re_{25}$ thermocouple (Nishihara et al., 2020). The dark blue shaded area indicates an allowed region for the Aki-Grt boundary. The solid dark represents the most likely transition curve within this range. The orange line on a top figure (a) indicates the Aki-Bdm phase transition boundary based on experimental data obtained in this study. The violet shaded area indicates an allowed region for the Aki-Bdm boundary for most experimental data points. The solid violet curve represents the most probable transition curve within this area. Dotted lines are result of linear extrapolation of the Aki-Bdm and Aki-Grt transition boundaries above 2,200 K. The dashed blue line indicates the Aki-Bdm phase transition boundary calculated from the proposed heat capacities difference (Figure S2 in Supporting Information S1). The dash dotted black curve is calculated Grt-Bdm boundary based on the slopes of Aki-Bdm and Grt-Aki boundaries at temperatures above 2,200 K.

$S_{Grt}-S_{Bdm}$ from the Equation 3 can be found from Equations 1 and 2:

$$S_{Aki} - S_{Bdm} = (dP/dT)_{Aki\text{-}Bdm} \times \Delta V_{Aki\text{-}Bdm} \quad (4)$$

$$S_{Grt} - S_{Aki} = (dP/dT)_{Grt\text{-}Aki} \times \Delta V_{Grt\text{-}Aki} \quad (5)$$

By summarizing Equations 4 and 5, we can express the difference in entropies of Grt and Bdm:

$$S_{Grt} - S_{Bdm} = (dP/dT)_{Aki\text{-}Bdm} \times \Delta V_{Aki\text{-}Bdm} + (dP/dT)_{Grt\text{-}Aki} \times \Delta V_{Grt\text{-}Aki} \quad (6)$$

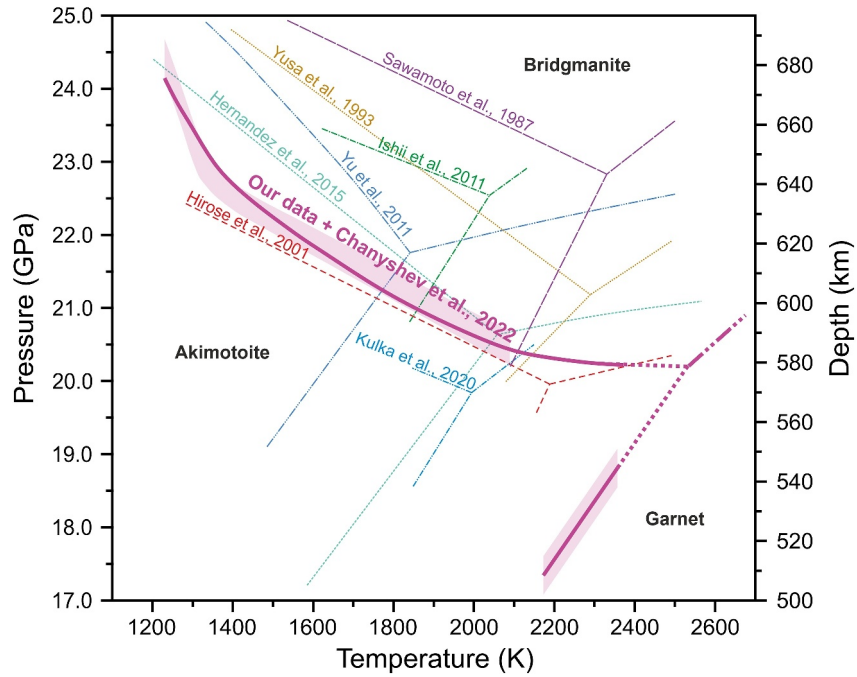

Figure 3. Comparison of our results with previous data in the $MgSiO_3$ system (Chanyshev et al., 2022; Hernández et al., 2015; Hirose et al., 2001; Ishii et al., 2011; Kulka et al., 2020; Sawamoto, 1987; Yu et al., 2011; Yusa et al., 1993). Current data combined with results from Chanyshev et al. (2022) are shown as solid violet curve. Dotted violet lines are result of linear extrapolation of the Aki-Bdm and Aki-Grt transition boundaries above 2200 K. The dash dotted black curve is calculated Grt-Bdm boundary based on the slopes of Aki-Bdm and Grt-Aki boundaries at temperatures above 2,200 K.

Therefore, the slope of the Grt-Bdm transition boundary is defined as:

$$(dP/dT)_{\text{Grt-Bdm}} = \left((dP/dT)_{\text{Aki-Bdm}} \times \Delta V_{\text{Aki-Bdm}} + (dP/dT)_{\text{Grt-Aki}} \times \Delta V_{\text{Grt-Aki}}\right)/\Delta V_{\text{Grt-Bdm}} \quad (7)$$

The volume changes of Aki-Bdm, Grt-Aki, and Grt-Bdm phase transitions can be determined from the experimentally investigated equations of state of $MgSiO_3$ Aki, Grt and Bdm. At around triple Aki-Grt-Bdm point, $\Delta V_{\text{Aki-Bdm}} \approx 1.05$ cm^3/mol, $\Delta V_{\text{Grt-Aki}} \approx 1.93$ cm^3/mol and $\Delta V_{\text{Grt-Bdm}} \approx 2.96$ cm^3/mol. The resulting $(dP/dT)_{\text{Grt-Bdm}}$ is positive and equals 5.5 MPa/K.

Figure 3 shows a comparison between the current results combined with those of Chanyshev et al. (2022) and the previous data obtained using multi-anvil apparatuses and in computational studies. The resulting Aki-Bdm boundary has a steep convex curve, and its slope gradually changes from −8.1 MPa/K at low temperatures up to 1,300 K to −0.6 MPa/K above 2,200 K. The curved Aki-Bdm boundary curvature is explained by different curvatures of the Aki and Bdm heat capacities with temperature, as discussed in Chanyshev et al. (2022). Here we propose variations in the Aki and Bdm heat capacities to 2,500 K based on our experimental data (Figure S2 in Supporting Information S1), and show how the Aki-Bdm boundary bends according to these variations (Figure 2b). The Aki heat capacity should be higher than that of Bdm in the temperature range of 850–2,400 K (Figure S2 in Supporting Information S1). This difference in curvature could result from temperature-dependent cation disorder in Aki, as discussed in Chanyshev et al. (2022).

The determined Clapeyron slope of the Aki-Bdm boundary at 2,200–2,350 K is less steep than that from the other experimental and computational studies, whereas the Clapeyron slope of the Grt-Aki boundary is similar to that from the previous studies (Hernández et al., 2015; Hirose et al., 2001; Ishii et al., 2011; Kulka et al., 2020; Sawamoto, 1987; Yu et al., 2011; Yusa et al., 1993). Our new data does not change the curvature of the combined Aki-Bdm boundary up to 2,100 K. Therefore, we do not discuss the variation in slope of this boundary at low temperatures here, since this was already discussed in Chanyshev et al. (2022). The proposed triple point of Aki-Bdm-Grt is located at higher temperature than previously suggested (Figure 3).

Of all the previous studies, the most similar results were obtained by Hirose et al. (2001). They also determined $MgSiO_3$ phase diagram using a multi-anvil apparatus and in situ X-ray diffraction, although their experimental procedure differed from the present study. They used X-ray only for the pressure determination in situ, whereas the stable phase was determined after quench and decompression by analyses of the recovered samples. On the other hand, we used X-ray to determine pressure and stable phase in situ simultaneously. Notably, the most important experiment where they observed Grt as a run product failed within 4 min, and the target pressure contained uncertainty (Hirose et al., 2001). We hypothesize that in this short run, the pressure significantly decreased after the Grt formation. In our experiments, pressure was significantly dropped from 19.8 to 18.4 GPa (−1.4 GPa) at ≈2,350 K and from 19.2 to 17.1 (−2.1 GPa) at 2,187 K during the formation of Grt from Aki sample at constant temperature. If the pressure in experiments from Hirose et al. (2001) was also significantly reduced (−1.4 to −2.1 GPa), then this means that the triple point should be at significantly higher temperatures, approximately at P-T conditions which we proposed (Figure S3 in Supporting Information S1).

3.2. D660 Topography in Plume Zones

The temperature beneath hotspots at around 660 km depth is approximately 200–300 K higher than the surrounding mantle (Karato, 1993; Katsura, 2022; White & McKenzie, 1995), leading to plume temperatures of 2,200–2,400 K at the topmost region of the lower mantle. Therefore, the $MgSiO_3$ transformation that we have determined at 2,200–2,350 K may control the topography of seismic discontinuities in mantle plume regions and also affect geodynamics. However, the Aki-Bdm and Aki-Grt transitions occur at about 580 and 530–570 km, respectively (Figure 4), but there are no detectable discontinuities in plume zones at these depths (Deuss et al., 2006). The most elevated D660 in mantle plume regions was detected at 630–640 km depth beneath Yellowstone (Schmandt et al., 2012).

A possible factor that can explain the discontinuity at such depths is an Al or Fe effect. At high temperatures, Bdm contains a significant amount of Al and Fe (Ishii et al., 2011; Ishii, Kojitani & Akaogi, 2018; Nishiyama & Yagi, 2003). Al-rich Bdm transforms to Grt at higher pressures than Al-free Bdm transforms to Aki (Kubo & Akaogi, 2000). At low Al content, Grt gradually transforms to Bdm via a binary loop, whereas at high Al content, Grt abruptly transforms to Bdm + corundum (Cor). However, the gradual Grt-Bdm transformation via binary loop cannot cause detectable seismic discontinuity, whereas the abrupt Grt-Bdm+Cor transition occurs at much greater depths than 660 km (Ishii et al., 2023).

In contrast to the Al effect, the Fe effect can explain the elevation of the 660-km discontinuity in plume zones. The Fe-rich Grt-Aki and Aki-Bdm transitions occur at higher pressures than the Fe-free transitions (Ohtani et al., 1991). In the pyrolite model, Bdm contains about 10% of Fe, and for this Fe content, the Aki-Bdm transition shifts to ≈ +1 GPa at 2,073 K relative to the Fe-free system (Ohtani et al., 1991). With a 10% of Fe content in Bdm, the Aki-Bdm transition occurs via a binary loop, but this loop is very narrow (Ohtani et al., 1991), and may therefore cause a sharp discontinuity, similar to ringwoodite dissociation in $(Mg_{90}Fe_{10})_2SiO_4$ system (Ishii et al., 2019). Shift of the Aki-Bdm transition boundary to a higher pressure can explain the possible discontinuity at around 600–610 km depth, but this is shallower than seismologically detected. The shift of this boundary to an even higher pressure can be caused by the combined effect of the Al and Fe, although it has not been experimentally investigated. However, this combined effect can cause the shift of the Grt-Bdm boundary to the lower temperatures, meaning that the discontinuity beneath plume zones is caused by the Grt-Bdm transition instead of the Aki-Bdm transition. The Grt-Bdm transition in an Fe-Al-rich system may occur gradually since this transition is topologically a binary loop in Fe-Mg-Si (Ohtani et al., 1991) and Al-Mg-Si (Kubo & Akaogi, 2000) systems, and a gradual transition cannot explain the discontinuity. Therefore, the Aki-Bdm transition in Al-Fe-rich system can cause a sharp discontinuity, unlike the Grt-Bdm transition in Fe-Al-rich system. However, all previous petrological studies have revealed that Aki is not a stable phase in pyrolytic system at the plume zone conditions, near the 660 km depth (Dong et al., 2025; Ishii et al., 2011; Nishiyama & Yagi, 2003).

Both the Aki-Bdm and Grt-Bdm transitions are associated with significant density change at 2,300–2,600 K, +5.5% and 11.8%, respectively (Figure S4 in Supporting Information S1). These changes are comparable with the +7.9% density change associated with the ringwoodite dissociation reaction in the average mantle (Yu et al., 2011). Taking all these factors into account, it is difficult to reach an unambiguous conclusion about which phase transition causes the seismic discontinuity beneath hotspots. Therefore, we will discuss the possible effect of both transitions on mantle convection in the next section.

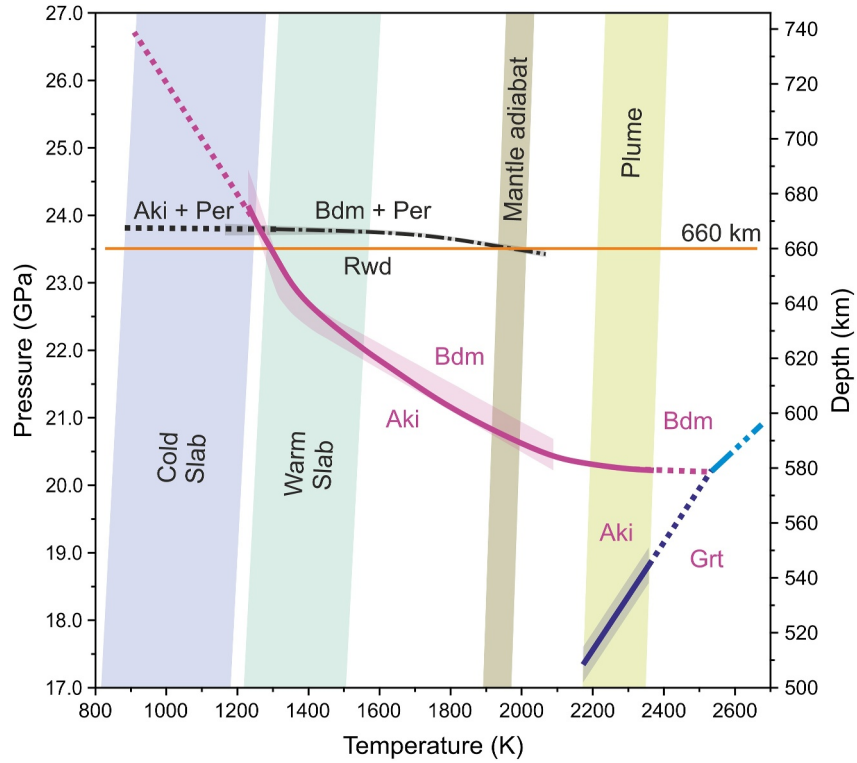

Figure 4. Combination of the present results with previous data from (Chanyshev et al., 2022) in MgO-SiO_2 systems. Cold and warm subduction geotherms are from (Ganguly et al., 2009; Thompson, 1992), and the average mantle geotherm is from (Katsura, 2022). The plume geotherm is drawn assuming that the temperatures in plumes are 200–300 K higher than the ambient mantle (Karato, 1993; Katsura, 2022; White & McKenzie, 1995). The horizontal solid orange line indicates 660 km depth (Dziewonski & Anderson, 1981). The Rwd dissociation boundary from (Chanyshev et al., 2022) is shown as a dot-dashed black curve and gray-shaded area. The Aki-Bdm transition boundary is shown by a solid violet curve. The Grt-Aki boundary is shown as solid dark blue curve and blue-shaded area. The dotted lines are the result of linear extrapolation of the Rwd dissociation boundary below 1,300 K, the Aki-Bdm boundary below 1,300 K and above 2,350 K, and the Aki-Grt boundary above 2,350 K. The dash double dotted blue line is the calculated Grt-Bdm boundary based on the slopes of Aki-Bdm and Grt-Aki boundaries at temperatures above 2,200 K. Aki, $MgSiO_3$ akimotoite; Bdm, $MgSiO_3$ bridgmanite; Per, MgO periclase; Rwd, Mg_2SiO_4 ringwoodite; Grt, $MgSiO_3$ majorite garnet.

3.3. Geodynamic Implications

The Clapeyron slope of the phase transition boundary of major mantle minerals affects mantle convection. If the dP/dT of a phase transition is positive or negative, the phase transition enhances or impedes mantle convection, respectively (Faccenda & Dal Zilio, 2017; Schubert et al., 1975). However, a recent geodynamic study found that the Clapeyron slope of the phase transition does not significantly impact global dynamics (Morgan et al., 2025). Nevertheless, we will estimate the possible effect of the determined phase transition slopes on mantle geodynamics.

The determined Aki-Bdm boundary in Al- and Fe-free system at 2,200–2400 K has an almost neutral slope (Figure 4), indicating that this transition has no effect on the mantle convection beneath plume zones. The well-known phenomenon of upwelling plumes is broadening and horizontal deflection around a depth of 1,000 km (French & Romanowicz, 2015; Lei et al., 2020). At around 660 km, some plumes tend to flatten and bend (Chang et al., 2016; Tosi & Yuen, 2011), but the change in plume shape is not necessarily associated with a Bdm-forming phase transition. In the case of the Samoan plume, plume bending is caused by interaction with the stagnant Tongo slab in the transition zone (Chang et al., 2016).

We also consider the possibility that the Grt-Bdm transition causes the discontinuity beneath hotspots. If the plume temperature is significantly higher than that proposed by Karato (1993), Katsura (2022), White and McKenzie (1995), and is approximately 500–600 K higher than the surrounding mantle, the Grt-Bdm transition

may occur and affect mantle convection. The calculated Grt-Bdm boundary slope is positive and equals 5.5 MPa/K. Therefore, it may impart an upward buoyancy to hot plumes and enhance their upwelling. It may contribute to the plume thinning at depths between 660 and 410 km, as observed beneath the Hawaiian hotspots (Agius et al., 2017).

4. Summary

We determined the $MgSiO_3$ phase diagram at 2,200–2,350 K and 17.4–20.3 GPa using advanced multi-anvil techniques with in situ X-ray diffraction. At these conditions, the Aki-Bdm boundary has an almost neutral slope of −0.6 MPa/K, whereas the Aki-Grt boundary has a steep positive slope of 8.8 MPa/K. The triple Aki-Bdm-Grt point is located at about 20.2 GPa and 2,530 K by the linear extrapolation of the Aki-Bdm and Aki-Grt boundaries. Based on the slopes of Aki-Bdm and Grt-Aki boundaries at temperatures above 2,200 K, we calculated the slope of the Grt-Bdm boundary as 5.5 MPa/K. Our results are comparable with those obtained by (Hirose et al., 2001), but the triple Aki-Bdm-Grt point was determined at a much higher temperature. We cannot unambiguously conclude which phase transition causes discontinuity beneath hotspots. Therefore, we discussed the possible effect of both Aki-Bdm and Grt-Bdm transitions on mantle convection. The Aki-Bdm transition may cause the elevated 660-km discontinuity beneath plume zones. However, the neutral slope of this transition has no effect on mantle convection beneath plume zones. In contrast, the Grt-Bdm transition may impart an upward buoyancy to hot plumes and enhance their upwelling, which contributes to the plume thinning between 660 and 410 km depths.

Conflict of Interest

The authors declare no conflicts of interest relevant to this study.

Data Availability Statement

The XRD data for this paper are given in Zenodo: Chanyshev (2025).

Acknowledgments
This work was funded by a research project approved by the European Research Council (ERC) under the European Union's Horizon 2020 research and innovation program (Proposal No. 787 527) to T. Katsura. We appreciate H. Fischer, S. Übelhack, R. Njul, A. Rother and U. Trenz at Bayerisches Geoinstitut and S. Sonntag at Deutsches Elektronen-Synchrotron (DESY) for their technical assistance. Open Access funding enabled and organized by Projekt DEAL.

References

Agius, M. R., Rychert, C. A., Harmon, N., & Laske, G. (2017). Mapping the mantle transition zone beneath Hawaii from Ps receiver functions: Evidence for a hot plume and cold mantle downwellings. *Earth and Planetary Science Letters*, *474*, 226–236. https://doi.org/10.1016/j.epsl.2017.06.033

Chang, S.-J., Ferreira, A. M., & Faccenda, M. (2016). Upper-and mid-mantle interaction between the Samoan plume and the Tonga–Kermadec slabs. *Nature Communications*, *7*(1), 10799. https://doi.org/10.1038/ncomms10799

Chanyshev, A. (2025). MgSiO3 HT XRD data [Dataset]. *Zenodo*. https://doi.org/10.5281/zenodo.16743398

Chanyshev, A., Ishii, T., Bondar, D., Bhat, S., Kim, E. J., Farla, R., et al. (2022). Depressed 660-km discontinuity caused by akimotoite–bridgmanite transition. *Nature*, *601*(7891), 69–73. https://doi.org/10.1038/s41586-021-04157-z

Chanyshev, A., Martirosyan, N., Wang, L., Chakraborti, A., Purevjav, N., Wang, F., et al. (2024). Thermal equation of state of cubic silicon carbide at high pressures. *ChemPhysChem*, *25*(9), e202300604. https://doi.org/10.1002/cphc.202300604

Deuss, A., Redfern, S. A., Chambers, K., & Woodhouse, J. H. (2006). The nature of the 660-kilometer discontinuity in Earth's mantle from global seismic observations of PP precursors. *Science*, *311*(5758), 198–201. https://doi.org/10.1126/science.1120020

Dong, J., Fischer, R. A., Stixrude, L. P., Brennan, M. C., Daviau, K., Suer, T.-A., et al. (2025). Nonlinearity of the post-spinel transition and its expression in slabs and plumes worldwide. *Nature Communications*, *16*(1), 1039. https://doi.org/10.1038/s41467-025-56231-z

Dziewonski, A. M., & Anderson, D. L. (1981). Preliminary reference Earth model. *Physics of the Earth and Planetary Interiors*, *25*(4), 297–356. https://doi.org/10.1016/0031-9201(81)90046-7

Faccenda, M., & Dal Zilio, L. (2017). The role of solid–solid phase transitions in mantle convection. *Lithos*, *268*, 198–224. https://doi.org/10.1016/j.lithos.2016.11.007

Farla, R., Bhat, S., Sonntag, S., Chanyshev, A., Ma, S., Ishii, T., et al. (2022). Extreme conditions research using the large-volume press at the P61B endstation, PETRA III. *Journal of Synchrotron Radiation*, *29*(2), 409–423. https://doi.org/10.1107/s1600577522001047

French, S. W., & Romanowicz, B. (2015). Broad plumes rooted at the base of the Earth's mantle beneath major hotspots. *Nature*, *525*(7567), 95–99. https://doi.org/10.1038/nature14876

Ganguly, J., Freed, A. M., & Saxena, S. K. (2009). Density profiles of oceanic slabs and surrounding mantle: Integrated thermodynamic and thermal modeling, and implications for the fate of slabs at the 660 km discontinuity. *Physics of the Earth and Planetary Interiors*, *172*(3–4), 257–267. https://doi.org/10.1016/j.pepi.2008.10.005

Hernández, E. R., Brodholt, J., & Alfè, D. (2015). Structural, vibrational and thermodynamic properties of Mg_2SiO_4 and $MgSiO_3$ minerals from first-principles simulations. *Physics of the Earth and Planetary Interiors*, *240*, 1–24.

Hirose, K., Komabayashi, T., Murakami, M., & Funakoshi, K. I. (2001). In situ measurements of the majorite-akimotoite-perovskite phase transition boundaries in $MgSiO_3$. *Geophysical Research Letters*, *28*(23), 4351–4354. https://doi.org/10.1029/2001gl013549

Houser, C., & Williams, Q. (2010). Reconciling Pacific 410 and 660 km discontinuity topography, transition zone shear velocity patterns, and mantle phase transitions. *Earth and Planetary Science Letters*, *296*(3–4), 255–266. https://doi.org/10.1016/j.epsl.2010.05.006

Irifune, T., Nishiyama, N., Kuroda, K., Inoue, T., Isshiki, M., Utsumi, W., et al. (1998). The postspinel phase boundary in Mg_2SiO_4 determined by in situ X-ray diffraction. *Science*, *279*(5357), 1698–1700. https://doi.org/10.1126/science.279.5357.1698

Ishii, T., Chanyshev, A., & Katsura, T. (2022). A new approach determining a phase transition boundary strictly following a definition of phase equilibrium: An example of the post-spinel transition in Mg_2SiO_4 system. *Minerals*, *12*(7), 820. https://doi.org/10.3390/min12070820

Ishii, T., Frost, D. J., Kim, E. J., Chanyshev, A., Nishida, K., Wang, B., et al. (2023). Buoyancy of slabs and plumes enhanced by curved post-garnet phase boundary. *Nature Geoscience*, *16*(9), 828–832. https://doi.org/10.1038/s41561-023-01244-w

Ishii, T., Huang, R., Fei, H., Koemets, I., Liu, Z., Maeda, F., et al. (2018). Complete agreement of the post-spinel transition with the 660-km seismic discontinuity. *Scientific Reports*, *8*(1), 6358. https://doi.org/10.1038/s41598-018-24832-y

Ishii, T., Huang, R., Myhill, R., Fei, H., Koemets, I., Liu, Z., et al. (2019). Sharp 660-km discontinuity controlled by extremely narrow binary post-spinel transition. *Nature Geoscience*, *12*(10), 869–872. https://doi.org/10.1038/s41561-019-0452-1

Ishii, T., Kojitani, H., & Akaogi, M. (2011). Post-spinel transitions in pyrolite and Mg_2SiO_4 and akimotoite–perovskite transition in $MgSiO_3$: Precise comparison by high-pressure high-temperature experiments with multi-sample cell technique. *Earth and Planetary Science Letters*, *309*(3–4), 185–197. https://doi.org/10.1016/j.epsl.2011.06.023

Ishii, T., Kojitani, H., & Akaogi, M. (2018). Phase relations and mineral chemistry in pyrolitic mantle at 1600–2200°C under pressures up to the uppermost lower mantle: Phase transitions around the 660-km discontinuity and dynamics of upwelling hot plumes. *Physics of the Earth and Planetary Interiors*, *274*, 127–137. https://doi.org/10.1016/j.pepi.2017.10.005

Ito, E., & Takahashi, E. (1989). Postspinel transformations in the system Mg_2SiO_4-Fe_2SiO_4 and some geophysical implications. *Journal of Geophysical Research*, *94*(B8), 10637–10646.

Karato, S. I. (1993). Importance of anelasticity in the interpretation of seismic tomography. *Geophysical Research Letters*, *20*(15), 1623–1626. https://doi.org/10.1029/93gl01767

Katsura, T. (2022). A revised adiabatic temperature profile for the mantle. *Journal of Geophysical Research: Solid Earth*, *127*(2), e2021JB023562. https://doi.org/10.1029/2021jb023562

Kubo, A., & Akaogi, M. (2000). Post-garnet transitions in the system $Mg_4Si_4O_{12}$–$Mg_3Al_2Si_3O_{12}$ up to 28 GPa: Phase relations of garnet, ilmenite and perovskite. *Physics of the Earth and Planetary Interiors*, *121*(1–2), 85–102. https://doi.org/10.1016/s0031-9201(00)00162-x

Kulka, B. L., Dolinschi, J. D., Leinenweber, K. D., Prakapenka, V. B., & Shim, S.-H. (2020). The bridgmanite–akimotoite–majorite triple point determined in large volume press and laser-heated diamond anvil cell. *Minerals*, *10*(1), 67. https://doi.org/10.3390/min10010067

Lei, W., Ruan, Y., Bozdağ, E., Peter, D., Lefebvre, M., Komatitsch, D., et al. (2020). Global adjoint tomography—model GLAD-M25. *Geophysical Journal International*, *223*(1), 1–21. https://doi.org/10.1093/gji/ggaa253

Morgan, G. T., Davies, J. H., Myhill, R., & Panton, J. (2025). On the global geodynamic consequences of different phase boundary morphologies. *Solid Earth*, *16*(4/5), 297–314. https://doi.org/10.5194/se-16-297-2025

Nishihara, Y., Doi, S., Kakizawa, S., Higo, Y., & Tange, Y. (2020). Effect of pressure on temperature measurements using WRe thermocouple and its geophysical impact. *Physics of the Earth and Planetary Interiors*, *298*, 106348. https://doi.org/10.1016/j.pepi.2019.106348

Nishiyama, N., & Yagi, T. (2003). Phase relation and mineral chemistry in pyrolite to 2200°C under the lower mantle pressures and implications for dynamics of mantle plumes. *Journal of Geophysical Research*, *108*(B5), 2255. https://doi.org/10.1029/2002jb002216

Ohtani, E., Kagawa, N., & Fujino, K. (1991). Stability of majorite (Mg,Fe)SiO_3 at high pressures and 1800°C. *Earth and Planetary Science Letters*, *102*(2), 158–166. https://doi.org/10.1016/0012-821x(91)90005-3

Sawamoto, H. (1987). Phase diagram of $MgSiO_3$ at pressures up to 24 GPa and temperatures up to 2200°C: Phase stability and properties of tetragonal garnet. *High-Pressure Research in Mineral Physics: A Volume in Honor of Syun-iti Akimoto*, *39*, 209–219. https://doi.org/10.1029/gm039p0209

Schmandt, B., Dueker, K., Humphreys, E., & Hansen, S. (2012). Hot mantle upwelling across the 660 beneath Yellowstone. *Earth and Planetary Science Lerichtters*, *331*, 224–236. https://doi.org/10.1016/j.epsl.2012.03.025

Schubert, G., Yuen, D. A., & Turcotte, D. L. (1975). Role of phase transitions in a dynamic mantle. *Geophysical Journal International*, *42*(2), 705–735. https://doi.org/10.1111/j.1365-246x.1975.tb05888.x

Tange, Y., Nishihara, Y., & Tsuchiya, T. (2009). Unified analyses for P-V-T equation of state of MgO: A solution for pressure-scale problems in high P-T experiments. *Journal of Geophysical Research*, *114*(B3), B03208. https://doi.org/10.1029/2008jb005813

Thompson, A. B. (1992). Water in the Earth's upper mantle. *Nature*, *358*(6384), 295–302. https://doi.org/10.1038/358295a0

Tosi, N., & Yuen, D. A. (2011). Bent-shaped plumes and horizontal channel flow beneath the 660 km discontinuity. *Earth and Planetary Science Letters*, *312*(3–4), 348–359. https://doi.org/10.1016/j.epsl.2011.10.015

White, R., & McKenzie, D. (1995). Mantle plumes and flood basalts. *Journal of Geophysical Research*, *100*(B9), 17543–17585. https://doi.org/10.1029/95jb01585

Yu, Y. G., Wentzcovitch, R. M., Vinograd, V. L., & Angel, R. J. (2011). Thermodynamic properties of $MgSiO_3$ majorite and phase transitions near 660 km depth in $MgSiO_3$ and Mg_2SiO_4: A first principles study. *Journal of Geophysical Research*, *116*(B2), B02208. https://doi.org/10.1029/2010jb007912

Yusa, H., Akaogi, M., & Ito, E. (1993). Calorimetric study of $MgSiO_3$ garnet and pyroxene: Heat capacities, transition enthalpies, and equilibrium phase relations in $MgSiO_3$ at high pressures and temperatures. *Journal of Geophysical Research*, *98*(B4), 6453–6460. https://doi.org/10.1029/92jb02862

References From the Supporting Information

Akaogi, M., & Ito, E. (1993). Refinement of enthalpy measurement of $MgSiO_3$ perovskite and negative pressure-temperature slopes for perovskite-forming reactions. *Geophysical Research Letters*, *20*(17), 1839–1842. https://doi.org/10.1029/93gl01265

Ashida, T., Kume, S., Ito, E., & Navrotsky, A. (1988). $MgSiO_3$ ilmenite: Heat capacity, thermal expansivity, and enthalpy of transformation. *Physics and Chemistry of Minerals*, *16*(3), 239–245. https://doi.org/10.1007/bf00220691

Nishida, K., Xie, L., Kim, E. J., & Katsura, T. (2020). A strip-type boron-doped diamond heater synthesized by chemical vapor deposition for large-volume presses. *Review of Scientific Instruments*, *91*(9), 095108. https://doi.org/10.1063/5.0011742

Sokolova, T. S., Dorogokupets, P. I., Litasov, K. D., Danilov, B. S., & Dymshits, A. M. (2018). Spreadsheets to calculate P–V–T relations, thermodynamic and thermoelastic properties of silicates in the $MgSiO_3$–MgO system. *High Pressure Research*, *38*(3), 193–211. https://doi.org/10.1080/08957959.2018.1465056